Multifocus tomographic algorithm for measuring optically thick specimens

Andrew D. Yablon

Interfiber Analysis, 8 Manns Hill Crescent, Sharon, Massachusetts 02067, USA (andrew_yablon@interfiberanalysis.com)

Received August 2, 2013; revised September 18, 2013; accepted September 24, 2013;
posted September 30, 2013 (Doc. ID 195134); published October 24, 2013

A novel tomographic algorithm for reconstructing the two-dimensional refractive index fluctuations of an optically thick phase object from one-dimensional projections acquired at a multiplicity of focal positions and a multiplicity of angular orientations is described. The new method is validated by measurements of multicore and microstructured optical fibers using interference microscopy. The method will benefit other transverse fiber measurement technologies and is broadly applicable to any tomographic reconstruction problem in which the transverse dimension of the specimen is substantially larger than the depth-of-field of the imaging system. © 2013 Optical Society of America

OCIS codes: (110.6960) Tomography; (060.2270) Fiber characterization; (060.2300) Fiber measurements.
http://dx.doi.org/10.1364/OL.38.004393

Tomography is typically accomplished with a highly collimated probe such as an x ray, or alternatively with a diffracting probe beam, such as an acoustic signal [1]. Recently, tomographic algorithms originally developed for these situations have been applied by many research groups to the important problem of measuring the refractive index distribution of nonazimuthally symmetric optical fibers [2–9]. The transverse projection of features in an azimuthally symmetric optical fiber, such as conventional single-mode optical fiber, is unchanged by any amount of rotation about its central axis whereas the transverse projection of features inside a nonazimuthally symmetric fiber, such as a polarization-maintaining (PM) optical fiber, will change substantially when it is rotated about its central axis. In all these investigations, relatively thick specimens (~100 μm diameter optical fibers) were imaged by objective lenses with limited depth-of-field (typically ~1 μm), yet the tomographic reconstruction algorithms did not account for defocusing of features situated far from the focal plane, and therefore such features were poorly rendered. In this Letter I present a new multifocus reconstruction algorithm that overcomes this limitation so that features far from the focal plane are more precisely rendered in the reconstruction. This algorithm is particularly useful for measuring the transverse refractive index geometry of multicore optical fiber, an important emerging class of optical fibers [10,11]. The algorithm has broader applications to the general problem of reconstructing a two-dimensional cross section of a specimen from one-dimensional projections when the specimen's transverse dimension greatly exceeds the depth-of-field of the imaging system.

Many novel optical fibers, including photonic crystal fibers (PCF), PM fibers, and multicore optical fibers, are nonazimuthally symmetric. Quantifying the refractive index and geometry of such fibers is critically important for understanding their performance and optimizing their manufacture [11]. Such fibers have been measured by transverse tomographic interference microscopy [3,4,7,8], quantitative phase microscopy [2,6,9], or diffraction tomography [5]. The tomographic reconstruction algorithms used for these investigations assumed that the depth-of-field of the imaging system encompassed the transverse dimension of the fiber. When refractive index inhomogeneities (i.e., cores, airholes, or stress-applying members) are limited to a few micrometers from the fiber's center, this assumption is satisfactory. However, the core separations of multicore fibers, the transverse diameter of PCF microstructure, and the separation of PM fiber stress-applying members are all typically of the order of several tens of micrometers, exceeding the depth-of-field of relevant microscope objectives by as much as 2 orders of magnitude.

Figure 1 schematically illustrates the effect of limited depth-of-field on optical path length measured on a three-core fiber, for example with an interference microscope [3,4,8,12]. It is seen that at each illustrated focal position, cores outside the focal plane are smeared. To fully appreciate the challenge of image reconstruction in this situation, it is crucial to recognize that in each projection the smeared, out-of-focus cores are superposed with the in-focus cores such that separating in-focus from out-of-focus components at any particular focal position is impossible. The new algorithm presented here overcomes this limitation and greatly expands the variety of optical fibers measurable by transverse interferometry

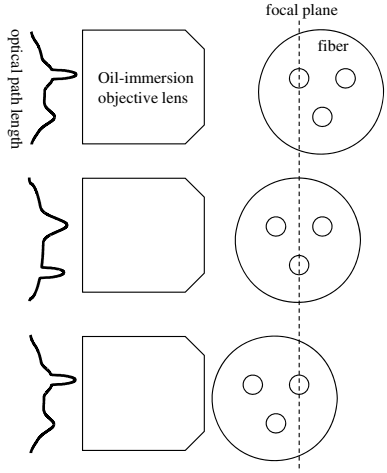

Fig. 1. Effect of focal position on measured optical path length when the specimen is larger than the imaging depth-of-field.

[3,4,7,8,12] and other transverse measurement techniques [2,5,6,9].

Conventional tomography acquires *single* projections of the specimen at a multiplicity of angular orientations and combines them together to form a complete two-dimensional cross section with the aid of the inverse Radon transform, which is efficiently computed via filtered backprojection [1,13]. By contrast, the new algorithm operates on a *set of projections* acquired at a multiplicity of focal positions, such as those depicted in Fig. 1.

Figure 2 illustrates how the sets of projections acquired at each angular orientation are combined. To simplify the discussion, consider a fiber with a single core located far from the fiber's center. A large set of one-dimensional projections is acquired as the fiber is scanned through the focal plane of the objective at a particular angular orientation. This can be rapidly accomplished at video rate by translating the fiber across the objective's focal plane at a fixed velocity. Each one-dimensional projection acquired at a particular focal plane and a particular angular orientation is then convolved with a filter function and the resulting set of one-dimensional filtered projections is reassembled into a two-dimensional matrix preserving the original orientation of acquisition. Filters applied during conventional filtered backprojection, such as a ramp filter in the spatial frequency domain [1] (also sometimes denoted as the Ramachandran–Lakshminarayanan filter [14]), are effective filter functions for the new algorithm.

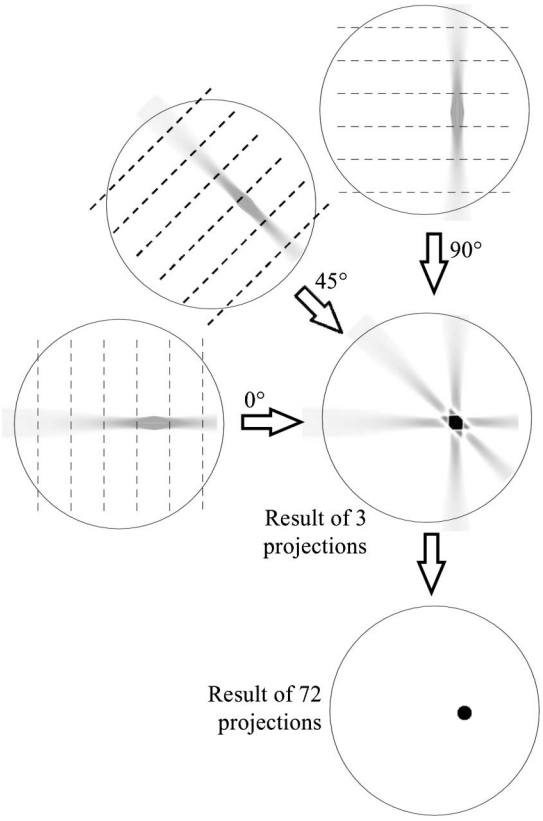

Fig. 2. Schematic illustration of new multifocus tomographic reconstruction algorithm applied to a single off-center core. The dashed lines schematically illustrate locations of (filtered) one-dimensional projections, each acquired at distinct focal plane locations. The collection of one-dimensional projections at a particular angular orientation comprise a two-dimensional matrix that is represented here as a gray-scale image (for brevity only the 0°, 45°, and 90° angles are shown here). The gray-scale images are accumulated in a final unified coordinate system as illustrated in this figure. Note that the gray-scale images produced by the new algorithm vary as a function of lateral position (parallel to the dashed lines) and also as a function of focal position (perpendicular to the dashed lines). Conventional filtered backprojection does not consider any variation with respect to focal position, so that the data comprising the gray-scale images does not vary as a function of focal position when performing conventional filtered backprojection. Compare to Figs. 25–17 of [13].

Figure 2 shows two-dimensional matrices associated with a few angular orientations after filtering. The dashed lines schematically illustrate locations of (filtered) one-dimensional projections acquired at distinct focal plane locations comprising the two-dimensional matrices. All of the reassembled matrices are superposed to yield the final reconstruction in a unified coordinate system. The spatial orientation of each measurement must be carefully preserved so that when the data is accumulated onto the final reconstruction, features acquired at each angular orientation correctly overlay with data acquired at other orientations. In other words, the center of rotation must correspond for all projections. As with conventional filtered backprojection, measurement artifacts are suppressed as the number of angular views in increased, and a more precise measurement results.

Figure 3 compares measurement of a multicore optical fiber (*Fibercore SM-4C1500*) using conventional filtered backprojection (a) to results using the new algorithm (b). Transverse interferometry [8,12] was performed at 850 nm for both cases at 72 angular locations every 5° over 360°. The experimental apparatus was previously described in [12]. No symmetry was assumed for these measurements. In this plot, the false color corresponds to Δn, the difference between the locally measured refractive index and the surrounding $n = 1.4610$ oil (*Cargille Labs* type 06350). The oil-immersion objective used to image the fiber had a numerical aperture of about 1.0, corresponding to a depth-of-field of the order of 1 μm or less. It is seen that conventional filtered backprojection smears the cores in the azimuthal direction because the fiber diameter of 125 μm exceeds this depth-of-field by more than 2 orders of magnitude. Furthermore, it is evident that the new algorithm has correctly captured evidence of a central dip or burn-off region inside the cores that is a vestige of the manufacturing process.

Images were acquired at video rate (19 frames per second) while the objective lens, tube lens, and two-dimensional silicon CCD array detector were held constant and the fiber was translated along the optical axis through the focal plane (as shown in Fig. 1) by a translation stage at a velocity of 25 μm per second. Two hundred distinct focal planes were acquired at video rate (at each of 72 distinct angular orientations) with a focal plane spacing of 1.3 μm corresponding to an effective depth-of-field of about 260 μm. Data acquisition required approximately 25 s per rotation angle and therefore approximately 30 min for the entire set of 72 angles. Data processing of all 14,400 phase images (72 angles by 200 frames/angle) require approximately 2 h using a

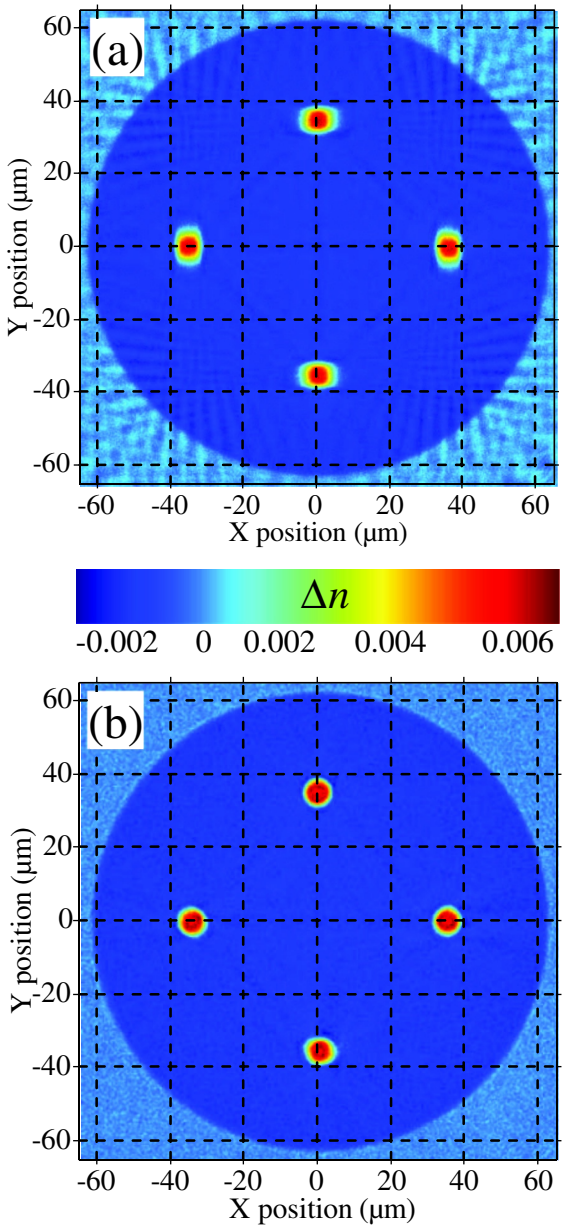

Fig. 3. Refractive index measurement of four-core multicore fiber reconstructed using (a) conventional filtered backprojection and (b) using the new algorithm. False color is Δn, the difference between the measured refractive index and the surrounding refractive index matching oil.

conventional desktop PC. This relatively coarse focal step size permitted a faithful rendering of the fiber while limiting the acquisition time and limiting the size of the dataset. Data was interpolated between the 1.3 μm focal step size to produce a step size of 0.154 μm matching the 0.154 μm corresponding to the pixel spacing of the image cast onto the silicon CCD detector. The cladding edges of the fiber were automatically detected by image processing and the center between these two edges defined the center of rotation one axis while the center of rotation in the orthogonal axis (focal axis) was found by determining the focal plane at which the cladding edges were most sharply resolved. In this way the center of rotation was automatically detected so that data corresponding to each angular orientation could be superposed with precise registration. It is notable that even with the relatively coarse angular grid of 5° increments, measurement artifacts at large radii are extremely weak.

Figure 4 shows a measurement of a single-mode air-silica microstructured optical fiber (*Thorlabs ESM-12B*) performed at a wavelength of 632.8 nm, but otherwise obtained under identical conditions as Fig. 3(b). The airholes in this fiber were filled with oil (*Cargille Labs* series AA) with a refractive index of 1.4540 while the surrounding oil was identical to Fig. 3. The refractive index of the internal oil, external oil, and pure silica cladding material ($n = 1.458$) is measured correctly. Moreover, aside from some weak measurement artifacts evident in the silica cladding material, the cladding refractive index is seen to be extremely uniform, as expected. No type of symmetry whatsoever was assumed for this measurement; any observed symmetry in the data is intrinsic to the fiber itself. There is some evidence of degraded accuracy in the measurement of the outer ring of holes, especially in the lower left quadrant. The spatial resolution of this measurement is estimated to be of the order of 1 μm across the entire microstructure. Compare Fig. 4 to recent measurements of a nearly identical fiber (*ESM-12-01*) in [5,9] to appreciate the significance and the effectiveness of the new algorithm.

This new multifocus tomography is applicable to any problem in which one-dimensional projections taken at multiple angles are synthesized into two-dimensional results in the presence of limited depth-of-field. Therefore, this approach can be expected to improve the performance of other fiber refractive index measurement techniques, such as quantitative phase microscopy [2,6,9], diffraction tomography [5], or residual stress measurement [7,9]. The discussion so far has concerned phase (optical path length) tomography, but the new algorithm should be equally effective for absorption tomography (as in medical x rays) or emission tomography [8]. Applications need not be limited to optical fiber characterization, and may include characterization of engineering materials, such as textile fibers or tomography of biomedical specimens contained within a capillary tube.

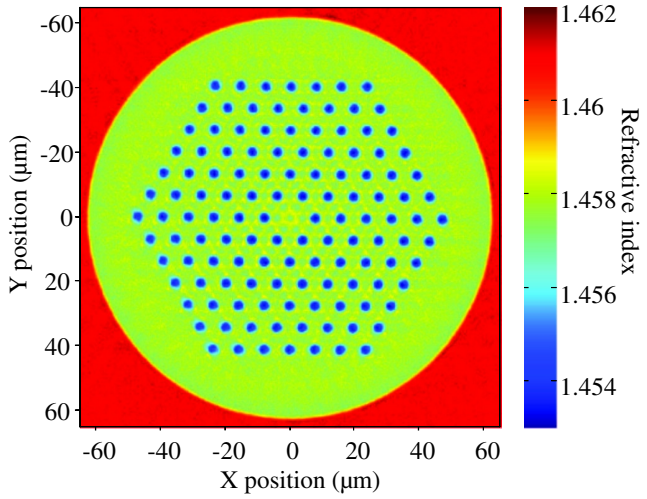

Fig. 4. Refractive index measurement of air-silica microstructured optical fiber at 632.8 nm.

In summary, I have described a new multifocus tomographic algorithm that produces superior results when the transverse dimension of a specimen exceeds the depth-of-field of the imaging system. Measurements of a multicore optical fiber and a microstructured optical fiber validate the efficacy of the method. In addition to measuring phase objects, such as optical fibers, the new tomographic algorithm may also be useful for absorption tomography or emission tomography as well as for biological or medical imaging applications.

The author acknowledges helpful discussions with Jayesh Jasapara.

References

1. A. C. Kak and M. Slaney, *Principles of Computerized Tomographic Imaging* (SIAM, 2001).
2. A. Barty, K. A. Nugent, A. Roberts, and D. Paganin, Opt. Commun. **175**, 329 (2000).
3. B. L. Bachim and T. K. Gaylord, Appl. Opt. **44**, 316 (2005).
4. B. L. Bachim, T. K. Gaylord, and S. C. Mettler, Opt. Lett. **30**, 1126 (2005).
5. W. Gorski and W. Osten, Opt. Lett. **32**, 1977 (2007).
6. N. M. Dragomir, X. M. Goh, and A. Roberts, Microsc. Res. Tech. **71**, 5 (2008).
7. P. Kniazewski, T. Kozacki, and M. Kujawinska, Opt. Lasers Eng. **47**, 259 (2009).
8. A. D. Yablon, Opt. Eng. **50**, 111603 (2011).
9. M. Jenkins and T. K. Gaylord, in *Frontiers in Optics 2012/ Laser Science XXVIII*, OSA Technical Digest (online) (Optical Society of America, 2012), paper FTh3C.2.
10. B. Zhu, T. F. Taunay, M. Fishteyn, X. Liu, S. Chandrasekhar, M. F. Yan, J. M. Fini, E. M. Monberg, and F. V. Dimarcello, Opt. Express **19**, 16665 (2011).
11. T. Hayashi, T. Taru, O. Shimakawa, T. Sasaki, and E. Sasaoka, Opt. Express **19**, 16576 (2011).
12. A. D. Yablon, IEEE J. Lightwave Technol. **28**, 360 (2010).
13. S. W. Smith, *The Scientists and Engineer's Guide to Digital Signal Processing* (California Technical Publishing, 1997).
14. G. N. Ramachandran and A. V. Lakshminarayanan, Proc. Natl. Acad. Sci. USA **68**, 2236 (1971).